Scripta Materialia 280 (2026) 117361

Contents lists available at ScienceDirect

Scripta Materialia

journal homepage: www.journals.elsevier.com/scripta-materialia

A novel specimen geometry for an improved estimation of hydrogen effects on the tensile behavior of face-centered cubic alloys

Si-Yeon Lee [a,†], Zhe Gao [a,†], Jae-Hyeok Choi [a], Yakai Zhao [b,c], Pei Wang [b,c], Kotaro Murakami [d], Shin-ichi Komazaki [d], Hyoung Seop Kim [e,f], Upadrasta Ramamurty [g,‡], Jae-il Jang [a,*]

[a] Division of Materials Science and Engineering, Hanyang University, Seoul 04763, Republic of Korea
[b] Future Energy Acceleration and Translation (FEAT), Agency for Science, Technology and Research (A*STAR), Singapore 138632, Singapore
[c] Institute of Materials Research and Engineering (IMRE), Agency for Science, Technology and Research (A*STAR), Singapore 138634, Singapore
[d] Department of Mechanical Engineering, Kagoshima University, Kagoshima 890-0065, Japan
[e] Graduate Institute of Ferrous & Eco Materials Technology, Pohang University of Science and Technology (POSTECH), Pohang 37673, South Korea
[f] Advanced Institute for Materials Research (WPI-AIMR), Tohoku University, Sendai 980-8577, Japan
[g] School of Mechanical and Aerospace Engineering, Nanyang Technological University, Singapore 639798, Singapore

ARTICLE INFO

Keywords:
Specimen geometry
Hydrogen
Electrochemical charging
Ag decoration
Uniaxial tensile properties

ABSTRACT

The significantly lower hydrogen (H) diffusivity in face-centered cubic (fcc) alloys compared to body-centered cubic alloys causes electrochemically charged H to remain primarily only in the near-surface region of tensile specimens. Such localized distribution often leads to a misinterpretation of H effect on the uniaxial tensile behavior of conventional specimens. To address this issue, here we propose a novel tensile specimen geometry for a better estimation of the influence of H on the tensile behavior of fcc alloys. Our results reveal that this new approach effectively captures H effects, which was confirmed by analyzing the H distribution within the specimens using the silver decoration technique.

Hydrogen (H) is well known to cause embrittlement or degrade mechanical performance (especially toughness and ductility) of metals and alloys [1–5]. Since it is a fundamental issue for structural materials that are susceptible to H exposure in various service environments, the influence of H on mechanical properties has long been investigated when new structural alloy is developed. For this reason, much research has recently been performed on the H effects in the research communities of high/medium-entropy alloys (H/MEAs) and additively manufactured alloys, both of which are relatively new members of the structural materials family [6–9]. Uniaxial tensile test is one of the most widely employed testing methods for examining the H-induced change in mechanical behavior [10,11]. There are two ways for the hydrogenation of tensile specimens: gaseous and electrochemical charging [12–14]. Of the two, the latter is relatively simple and easy to set up, making it more popularly adopted in lab-scale experiments.

Surface-absorbed H diffuses rapidly into the bulk. However, diffusivity depends significantly on the crystal structure of alloys: face-centered cubic (fcc) alloys exhibit higher H solubility but much lower H diffusivity than body-centered cubic (bcc) alloys [1,15,16]. Thus, in electrochemical hydrogen charging of a fcc alloy tensile specimen, H diffusion is likely to be confined near the surface of the specimen [17,18]. Such a non-uniform distribution can lead to an underestimation or misinterpretation of H effects on the uniaxial tensile properties of fcc alloys, as the tensile response is governed by the H-free bulk. With this in mind, as the first step to explore the effects of H in the additively manufactured CoCrNi MEA, here we propose a novel geometry of tensile specimen to more accurately examine the H effects. This new geometry introduces a groove (which differs from the conventional specimen geometries prescribed in the tensile testing standards such as ASTM-E8) while uniaxial loading condition is still maintained. The effectiveness of the suggested approach is verified by comparing the results with those obtained with the conventional geometry specimen.

* Corresponding author.
E-mail address: jijang@hanyang.ac.kr (J.-i. Jang).
† These authors contributed equally to this work.
‡ Upadrasta Ramamurty was an Editor of the journal during the review period of the article. To avoid a conflict of interest, Upadrasta Ramamurty was blinded to the record and another editor processed this manuscript.

https://doi.org/10.1016/j.scriptamat.2026.117361
Received 11 March 2026; Received in revised form 14 April 2026; Accepted 21 April 2026
Available online 22 April 2026

The examined CoCrNi MEA is fabricated via laser powder bed fusion (LPBF) process using TruPrint 1000 (TRUMPF, Germany) with layer thickness, laser power, hatch spacing, and scan speed of 30 μm, 150 W, 30 μm, and 670 mm/s, respectively. Microstructural characterization was conducted using electron backscattered diffraction (EBSD; Symmetry S3, Oxford Instruments, UK). Fig. 1 shows representative EBSD inverse pole figure (IPF) and phase maps obtained from the surface perpendicular to the build direction (BD) of the sample. The average grain size of the single fcc phase sample is found to be ~24.7 μm.

Tensile specimens were cut from the LPBF block by wire electrical discharge machining in the scanning direction (as shown in Fig. S1 of Supplementary Material, SM) and then mechanically polished (with sandpapers of grit number up to 2000). Tensile tests were performed using a universal testing machine (MINOS-001, MTDI, Korea) at room temperature (RT) under a slow strain rate of 10^{-4} s^{-1} similar to those in previous works [19,20]. The digital image correlation (DIC) technique was utilized to quantify strain values using Aramis software (GOM, Germany). Note that DIC measurements for the novel (U-grooved) specimens were performed on the outer flat surface because the concave geometry in the grooved side limits a reliable DIC analysis.

H was electrochemically pre-charged at RT using a potentiostat/galvanostat equipment (CS2150, Corrtest, China) in a 0.1 M NaOH solution containing 5 g/L NH_4SCN under a constant current density of 100 mA/cm^2 for 72 h. All the tensile tests were started within 20 min after H-charging to minimize any potential effect of H outgassing. Fracture surfaces were observed using scanning electron microscopy (SEM; Apreo S Hivac, Thermo Fisher Scientific, USA).

The amount of absorbed H was measured by thermal desorption spectroscopy (TDS) analysis using a gas chromatographer (JTF-20A, J-Science Lab, Japan). For TDS, the H-charged sample was heated to 400 °C at a constant heating rate of 100 °C/h. In addition, for confirming the H distribution within the specimen, Ag decoration [21,22] was performed by immersing the specimen in an aqueous solution with 4.3 mmol/L $Ag[K(CN)_2]$ for 5 min.

Fig. 2 shows representative results from the tensile tests of the LPBF-fabricated MEA specimens (with the conventional geometry shown) in uncharged and H-charged conditions. No significant differences were observed in the ultimate tensile strength (772 ± 0.7 and 727 ± 7.8 MPa for uncharged and H-charged specimen, respectively) and elongation to failure (15.3 ± 1.4% and 13.7 ± 0.2% for uncharged and H-charged specimen, respectively) between the two conditions. The DIC results indicate that the local strain distributions and magnitudes are generally comparable. The variations in the work hardening rate with strain are also similar. All these results suggest that the uniaxial tensile behavior of the alloy is not markedly affected by H. However, considering the low diffusivity of H in fcc samples and thus the possibility that electrochemically charged H atoms can exist only near the surfaces of fcc specimens, this observed H effect is possibly an experimental artefact. This possibility was confirmed by post-mortem fractographic analysis

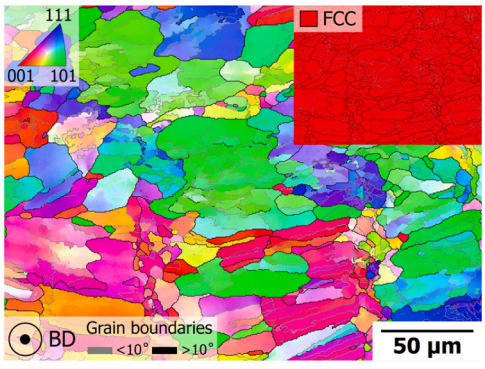

Fig. 1. Representative example of EBSD Inverse pole figure (IPF) map (with inset of phase map).

using SEM that was conducted in both the center and near-edge regions of the tested specimens. As shown in Fig. 2, the uncharged specimen exhibits only ductile features of dimples in all regions, whereas the H-charged specimen shows both brittle and ductile fracture features depending on the location examined (i.e., only the region near the surface for the former and most of the interior for the latter), indicating that the influence of electrochemically charged H is confined to the regions near the specimen surface.

The H concentration profile within the electrochemically H-charged specimen can be estimated by the Fick's second law [23,24]:

$$C(x,\ t_c) = C_s\left[1 - erf\left(\frac{x}{2\sqrt{D_H t_c}}\right)\right] \quad (1)$$

where C_s is the H concentration at the surface, t_c is the charging time, and D_H is the hydrogen's diffusion coefficient. For D_H a value of 1.0×10^{-15} m^2/s, which is estimated from H permeation tests of conventionally manufactured CoCrNi alloys at RT [25], is used. C_s is given by the relation:

$$C_s = \frac{w \cdot C_M}{4}\sqrt{\frac{\pi}{D_H t_c}} \quad (2)$$

where w is the sample thickness (1 mm), C_M is the average H content in the sample. Value of C_M determined using TDS is shown in the inset of Fig. 3. The average H content estimated from the desorption curve is ~15.7 wppm. The normalized H concentration profile in the H-charged sample, calculated using Eqs. (1) and (2), is shown in Fig. 3, indicating that electrochemically charged H atoms are concentrated primarily near the charged surface (within several tens of micrometers from the surface). The H penetration depth is significantly smaller than the thickness of the tensile specimen with conventional geometry displayed in Fig. 2, implying that the H effect obtained with such a specimen may not accurately reflect the actual susceptibility of the alloy.

One may imagine that this issue (originates from the low hydrogen diffusivity) can be overcome by extending the charging time t_c and/or by increasing the charging current density (and thus the average H content C_M) to enhance H penetration depth. However, both approaches have a limited influence on the penetration depth, which can be estimated using Eqs. (1) and (2). For example, doubling t_c (from 72 to 144 h) results in a marginal increase in the penetration depth from ~73 to ~101 μm. Likewise, doubling C_M (from ~15.7 to ~31.4 wppm) changes it only from ~73 to ~78 μm. This suggests that controlling the conditions of electrochemical charging cannot fundamentally resolve the challenge associated with the near-surface localization of hydrogen in the fcc alloys. Therefore, alternative approaches are necessary.

In the case of gaseous H-charging, introduction of an inner hole into round-bar-type tensile specimens was reported to improve testing efficiency [26,27]. However, applying such a geometry to electrochemical charging cases may require a rather complex charging system capable of introducing and maintaining electrolyte inside the inner hole. Considering these limitations, the present study proposes a novel tensile specimen geometry to enable an improved evaluation of surface-localized H effects in fcc alloys in lab-scale experiments.

The most crucial requirement for the novel geometry of tensile specimen is to maintain a uniaxial condition; that is, the entire gauge section of a specimen has a uniform stress state having a single normal stress component, which is possible only by keeping the cross-sectional area of the gauge section constant along the loading direction. To satisfy this simple but important requirement, as shown in Fig. 4, we introduced the U-groove into the tensile specimen to maintain a constant cross-sectional area while allowing electrochemically charged H to penetrate more deeply into the specimen interior compared to the conventional specimen. In particular, the ligament thickness is designed to be ~100 μm to allow H to reach the mid-thickness of the ligament, as illustrated with the H diffusion depth profile in Fig. 3.

To verify that the stress state in the designed specimen corresponds

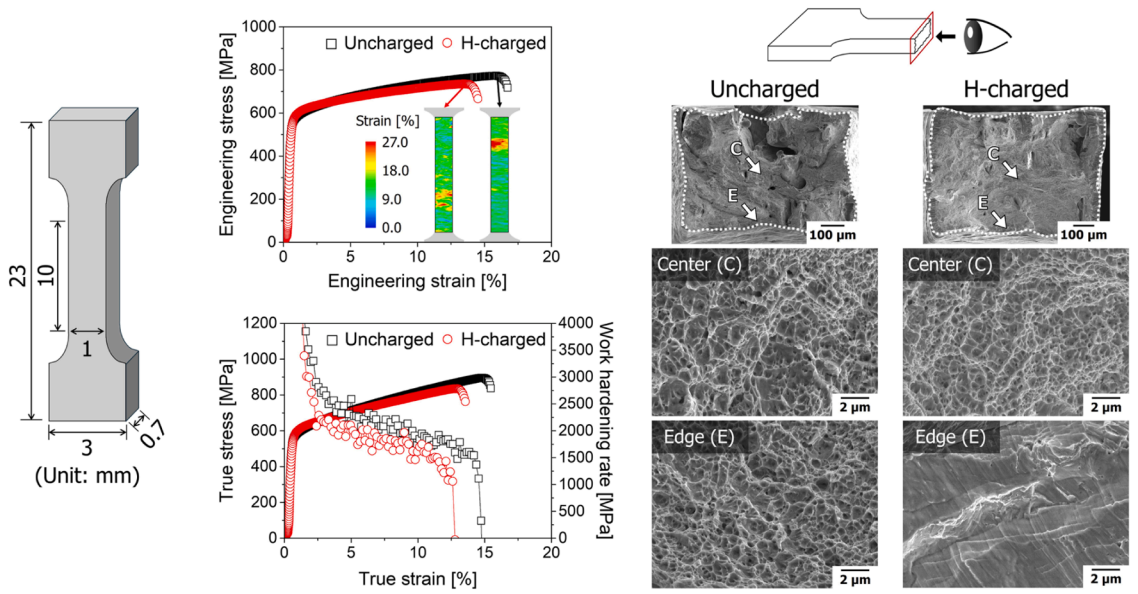

Fig. 2. (left) Adopted conventional geometry of tensile specimen. (middle) Results from the tensile tests (with the inset showing strain distribution measured using DIC). (right) SEM images of the fracture surfaces of tensile-tested specimens.

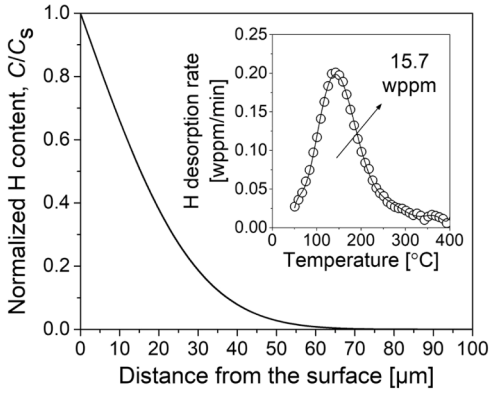

Fig. 3. Estimated H distribution in H-charged specimens (with the inset showing the spectra obtained from TDS).

to that of the uniaxial tensile condition, tensile tests were conducted using the uncharged specimens having conventional and novel geometries, and the results are compared in Fig. S2 of the SM. Both specimens exhibit similar engineering stress–strain curves except for a slightly higher yield strength for the novel specimen. Such a marginal increase in strength may be attributed to a thin hardened surface layer produced during the introduction of the U-groove by electrical discharge machining [28]. The results from the finite element analysis, displayed in Fig. S3 of SM, confirm the stress distribution is uniform in the gauge section of novel specimen during tensile loading.

Representative results from tensile tests using the novel geometry specimens are provided in Fig. 4. The H-charged specimen exhibits a pronounced reduction in the ultimate tensile strength (826 ± 12.6 and 726 ± 6.1 MPa for uncharged and H-charged specimens, respectively) and elongation (16.6 ± 0.6% and 8.1 ± 0.2% for uncharged and H-charged specimens, respectively) compared to the uncharged counterpart, which is markedly different from that obtained with the conventional geometry specimens. The DIC results (in the inset of Fig. 4) reveal that localized deformation in the H-charged specimen initiates within the ligament region at a much lower strain level than that in the case of the uncharged specimen. Consistent with this observation, a sudden decrease in the work hardening rate prior to the initiation of necking is noteworthy, implying a pronounced embrittlement behavior. This trend is also confirmed by fractographic analysis. While the uncharged specimen exhibits ductile failure features only with dimples, the H-charged specimen shows notably extensive brittle fracture features throughout the ligament region, implying that the tensile behavior of the H-charged specimen is mainly affected by H.

To examine the above scenario, the through-thickness distribution of H in the ligament of H-charged specimens was analyzed using the Ag decoration technique [21,22]. Although this simple chemical method does not provide a quantitative measure of the H concentration, it enables visualization of the spatial distribution of "diffusible" H. During the decoration experiment, the H atoms (absorbed on the specimen surface) reduce Ag^+ ions to elemental Ag through the reaction, $Ag^+ + H \rightarrow Ag + H^+$, and thus the sites where white Ag particles are observed can be considered as the H trapping ones. Fig. 5 shows both the schematics of the Ag decoration procedure for the H-charged specimen and the corresponding SEM images together with those of the uncharged specimen for comparison. Since H can penetrate from all the exposed surfaces during electrochemical charging, the upper surface of the H-charged specimens was subsequently polished (for ~200 μm reduction) after charging to exclude the contribution of H diffused from the top surface and thereby analyze the through-thickness H distribution in the ligament. For the uncharged specimen, only a few Ag particles are observed on the surface, likely associated with the pre-existing H. In contrast, the H-charged specimen exhibits a substantially higher density of Ag particles not only near the edge (regions A and C) but at the center of the ligament (region B) as well. This observation indicates that H is indeed broadly distributed throughout the ligament, which supports the tensile behavior and fractographic features of the H-charged specimen in Fig. 4.

In summary, we propose a novel geometry of tensile specimen to more accurately examine the H effects on tensile behavior of fcc alloys such as LPBF-fabricated MEA examined in this study. Due to the limited H penetration depth confined to the near-surface region of fcc alloys, H effects are not distinctly captured in tensile results obtained with conventional geometry specimens. Tensile results obtained with the novel geometry specimen clearly captured the H effects. This finding was experimentally confirmed by analyzing the H distribution within the novel geometry specimens using the Ag decoration technique.

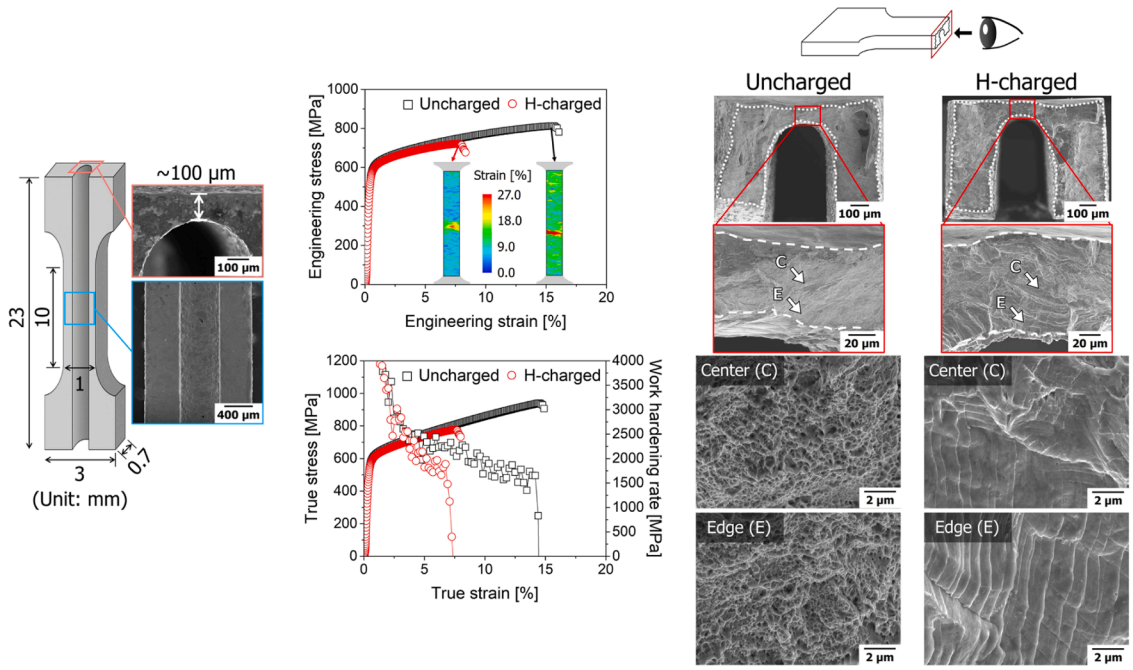

Fig. 4. (left) Suggested novel geometry of tensile specimen. (middle) Results from the tensile tests (with the inset showing strain distribution measured using DIC). (right) SEM images of the fracture surfaces of tensile-tested specimens.

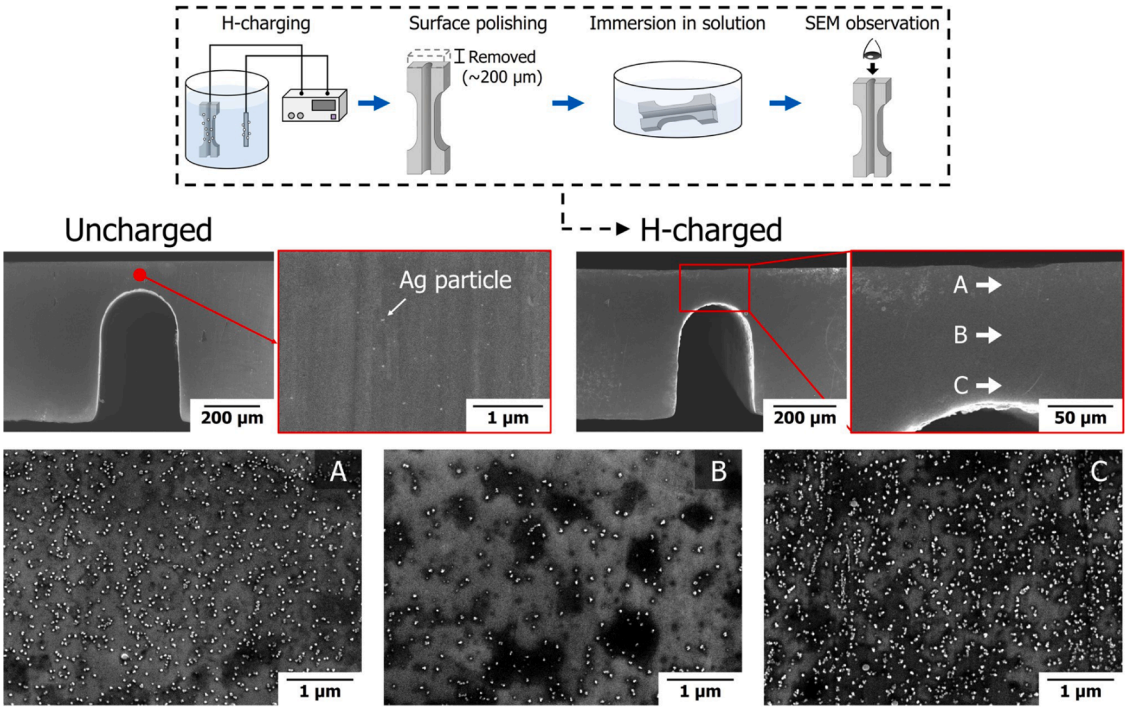

Fig. 5. (upper) Schematic illustration of Ag decoration procedure for H-charged specimens. (lower) Representative SEM images of the uncharged and H-charged samples obtained from the ligament region, where A–C correspond to high-magnification views of the specific regions indicated in the H-charged sample.

CRediT authorship contribution statement

Si-Yeon Lee: Writing – original draft, Visualization, Investigation. **Zhe Gao:** Visualization, Validation, Data curation. **Jae-Hyeok Choi:** Investigation. **Yakai Zhao:** Resources, Investigation. **Pei Wang:** Resources, Investigation. **Kotaro Murakami:** Data curation. **Shin-ichi Komazaki:** Data curation. **Hyoung Seop Kim:** Funding acquisition, Validation. **Upadrasta Ramamurty:** Writing – review & editing. **Jae-il Jang:** Writing – review & editing, Funding acquisition, Conceptualization.

Declaration of competing interest

The authors declare that they have no known competing financial interests or personal relationships that could have appeared to influence the work reported in this paper.

Acknowledgements

The work at Hanyang University was supported by the National Research Foundation of Korea (NRF) grant funded by the Korea government (MSIT) (No. 2022R1A5A1030054 and RS-2026-25478573). The work at Kagoshima University was supported by JSPS KAKENHI Grant-in-Aid for Scientific Research (B), Grant Number 25K01124. The work at POSTECH was supported by the NRF grant funded by the MSIP (No. 2021R1A2C3006662 and 2022R1A5A1030054). UR and YZ would like to thank the support by A*STAR via Advanced Alloys and Coatings for Structural and Functional Applications in Extreme Environments project (Grant No. M25P1a0081). The authors appreciate Prof. Young-Chun Kim and Ji-Hyeon Kim for conducting FEA.

Supplementary materials

Supplementary material associated with this article can be found, in the online version, at doi:10.1016/j.scriptamat.2026.117361.

References

[1] S.P. Lynch, in: V.S. Raja, T. Shoji (Eds.), Stress Corrosion Cracking, Woodhead Publishing, Cambridge, 2011, pp. 90–130.
[2] Y. Zhao, D.-H. Lee, M.-Y. Seok, J.-A. Lee, M.P. Phaniraj, J.-Y. Suh, H.-Y. Ha, J.-Y. Kim, U. Ramamurty, J.-i. Jang, Resistance of CoCrFeMnNi high-entropy alloy to gaseous hydrogen embrittlement, Scr. Mater. 135 (2017) 54–58.
[3] S.K. Dwivedi, M. Vishwakarma, Hydrogen embrittlement in different materials: a review, Int. J. Hydrog. Energy 43 (2018) 21603–21616.
[4] H.-C. Shin, S.-G. Kim, B. Hwang, Comparative study of hydrogen embrittlement of tempered martensitic steels containing Ti, Nb and V, Met. Mater.-Int. 31 (2025) 1891–1901.
[5] S.-G. Kim, B. Hwang, Effect of Si on cementite morphology and hydrogen embrittlement resistance of tempered martensitic steels, Met. Mater.-Int. 31 (2025) 1313–1322.
[6] C.K. Soundararajan, H. Luo, D. Raabe, Z. Li, Hydrogen resistance of a 1 GPa strong equiatomic CoCrNi medium entropy alloy, Corrosion Sci. 167 (2020) 108510.
[7] J.-M. Park, Y. Zhao, T. Voisin, D.-H. Lee, S. Komazaki, Y. Ko, D. Kim, J.-Y. Suh, H. N. Han, Y.M. Wang, U. Ramamurty, J.-i. Jang, Hydrogen uptake and its influence in selective laser melted austenitic stainless steel: a nanoindentation study, Scr. Mater. 194 (2021) 113718.
[8] Y. Zhao, J.-M. Park, K. Murakami, S. Komazaki, M. Kawasaki, K. Tsuchiya, J.-Y. Suh, U. Ramamurty, J.-i. Jang, Exploring the hydrogen absorption and strengthening behavior in nanocrystalline face-centered cubic high-entropy alloys, Scr. Mater. 203 (2021) 114069.
[9] Z. Gao, D.-H. Lee, Y. Zhao, P. Wang, K. Murakami, S. Komazaki, J.-Y. Suh, H. S. Kim, U. Ramamurty, J.-i. Jang, Hydrogen trapping and micromechanical behavior in additively manufactured CoCrFeNi high-entropy alloy in as-built and pre-strained conditions, Acta Mater. 271 (2024) 119886.
[10] D.H. Lee, J.Y. Jung, K.H. Lee, S.Y. Lee, Y. Zhao, K.B. Lau, P. Wang, U. Ramamurty, Distinct effects of in-situ and ex-situ hydrogen charging methods on the mechanical behavior of CoCrFeNi high-entropy alloy fabricated by laser-powder bed fusion, J. Alloy. Compd. 940 (2023) 168858.
[11] S.-H. Li, D.-H. Lee, Y. Zhao, U. Ramamurty, Hydrogen-induced softening and embrittlement in 316L stainless steel fabricated using laser-powder bed fusion, Acta Mater. 274 (2024) 119959.
[12] C.San Marchi, B.P. Somerday, S.L. Robinson, Permeability, solubility and diffusivity of hydrogen isotopes in stainless steels at high gas pressures, Int. J. Hydrog. Energy 32 (1) (2007) 100–116.
[13] K. Verbeken, in: R.P. Gangloff, B.P. Somerday (Eds.), Gaseous Hydrogen Embrittlement of Materials in Energy Technologies, Woodhead Publishing, Cambridge, 2012, pp. 31–33.
[14] Y. Zhao, M.-Y. Seok, I.-C. Choi, Y.-H. Lee, S.-J. Park, U. Ramamurty, J.-Y. Suh, J.-i. Jang, The role of hydrogen in hardening/softening steel: influence of the charging process, Scr. Mater. 107 (2015) 46–49.
[15] F. Wei, K. Tsuzaki, in: R.P. Gangloff, B.P. Somerday (Eds.), Gaseous Hydrogen Embrittlement of Materials in Energy Technologies, Woodhead Publishing, Cambridge, 2012, pp. 493–525.
[16] Z. Gao, Y. Zhao, J.-M. Park, A.-H. Jeon, K. Murakami, S. Komazaki, K. Tsuchiya, U. Ramamurty, J.-i. Jang, Decoupling the roles of constituent phases in the strengthening of hydrogenated nanocrystalline dual-phase high-entropy alloys, Scr. Mater. 210 (2022) 114472.
[17] A.-M. Brass, J. Chêne, Hydrogen uptake in 316L stainless steel: consequences on the tensile properties, Corrosion Sci. 48 (10) (2006) 3222–3242.
[18] Y. Zhao, J.-M. Park, D.-H. Lee, E.J. Song, J.-Y. Suh, U. Ramamurty, J.-i. Jang, Influences of hydrogen charging method on the hydrogen distribution and nanomechanical properties of face-centered cubic high-entropy alloy: a comparative study, Scr. Mater. 168 (2019) 76–80.
[19] H. Luo, S.S. Sohn, W. Lu, L. Li, X. Li, C.K. Soundararajan, W. Krieger, Z. Li, D. Raabe, A strong and ductile medium-entropy alloy resists hydrogen embrittlement and corrosion, Nat. Commun. 11 (2020) 3081.
[20] Y. Zhou, W. Wu, J. Li, Simultaneous improvement of hydrogen embrittlement resistance and tensile strength of quenching and partitioning steel through dense multiple interfaces, Int. J. Hydrog. Energy 58 (2024) 1372–1385.
[21] Z. Tarzimoghadam, M. Rohwerder, S.V. Merzlikin, A. Bashir, L. Yedra, S. Eswara, D. Ponge, D. Raabe, Multi-scale and spatially resolved hydrogen mapping in a Ni–Nb model alloy reveals the role of the δ phase in hydrogen embrittlement of alloy 718, Acta Mater. 109 (2016) 69–81.
[22] J. Ovejero-García, Hydrogen microprint technique in the study of hydrogen in steels, J. Mater. Sci. 20 (1985) 2623–2629.
[23] J. Crank, The Mathematics of Diffusion, Oxford University Press, London, 1975. Second ed.
[24] A.E. Pontini, J.D. Hermida, X-ray diffraction measurement of the stacking fault energy reduction induced by hydrogen in an AISI 304 steel, Scr. Mater. 37 (11) (1997) 1831–1837.
[25] D.C. Yang, K.J. Kim, G. Lee, S.Y. Song, J.-H. Baek, J.-Y. Suh, S.-M. Seo, Y.K. Kim, Y. S. Na, S.S. Sohn, Roles of lattice and grain boundary on hydrogen diffusion and trap behaviors in single-and poly-crystalline CrCoNi medium-entropy alloy, J. Mater. Res. Technol-JMRT 31 (2024) 3971–3981.
[26] T. Freitas, F. Konert, J. Nietzke, Z. Krzysch, T. Böllinghaus, T. Michler, K. Wackermann, H. Oesterlin, M. Tlili, P. Ruchti, D. Beitelschmidt, S. Elsen-Humberg, T. Koenigs, T. Systermans, O. Sobol, Tensile testing in high-pressure gaseous hydrogen using the hollow specimen method, MRS Bull. 49 (2024) 1112–1120.
[27] F. Konert, F. Wieder, J. Nietzke, D. Meinel, T. Böllinghaus, O. Sobol, Evaluation of the impact of gaseous hydrogen on pipeline steels utilizing hollow specimen technique and μCT, Int. J. Hydrog. Energy 59 (2024) 874–879.
[28] J. Guo, M. Goh, Z. Zhu, X. Lee, M.L.S. Nai, J. Wei, On the machining of selective laser melting CoCrFeMnNi high-entropy alloy, Mater. Des. 153 (2018) 211–220.